

# Encoding Domain Knowledge in Multi-view Latent Variable Models: A Bayesian Approach with Structured Sparsity

Arber Qoku<sup>1,2</sup> and Florian Buettner<sup>1,2,3</sup>

<sup>1</sup>German Cancer Consortium (DKTK) and German Cancer Research Center (DKFZ)

<sup>2</sup>Goethe University Frankfurt, Germany

<sup>3</sup>Frankfurt Cancer Institute, Germany

{arber.qoku, florian.buettner}@dkfz.de

## Abstract

Many real-world systems are described not only by data from a single source but via multiple data views. For example, in genomic medicine, a patient can be described by data from different molecular layers. This raises the need for multi-view models that are able to disentangle variation within and across data views in an interpretable manner. Latent variable models with structured sparsity are a commonly used tool to address this modeling task but interpretability is cumbersome since it requires a direct inspection and interpretation of each factor via a specialized domain expert. Here, we propose MuVI, a novel approach for domain-informed multi-view latent variable models, facilitating the analysis of multi-view data in an inherently explainable manner. We demonstrate that our model (i) is able to integrate noisy domain expertise in form of feature sets, (ii) is robust to noise in the encoded domain knowledge, (iii) results in identifiable factors and (iv) is able to infer interpretable and biologically meaningful axes of variation in a real-world multi-view dataset of cancer patients.

## 1 Introduction

In many real-world applications, complex systems are characterized via multiple data views. That is, observations are represented by multiple groups of distinct features. These groups of features often represent different and complementary input sources that are required for a comprehensive characterization of a sample. For example, in genomic medicine, a patient can be described by quantifying different molecular layers such as the proteome, the microbiome and the transcriptome.

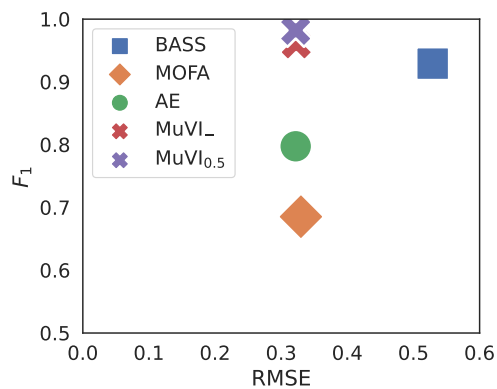


Figure 1: Performance of our model (MuVI) against competitive models. Only our model achieves a higher  $F_1$  score for recovering true active features while maintaining a low reconstruction error.

Latent variable models are powerful statistical tools that uncover the axes of variation between samples and data-views, by inferring unobserved hidden states from the observable high-dimensional data. To disentangle the sources of heterogeneity driving intra-view and inter-view variation in a meaningful manner, it is key that latent variable models are expressive and interpretable. Modeling approaches with the highest expressive power are based on variational autoencoders[Ainsworth et al., 2018] or Gaussian Process Latent Variable models [Damianou et al., 2012]. However, the non-linearities introduced to ensure a high expressive power hinder interpretability to the extent that linear approaches remain the dominant tool to analyze complex multi-view data in many domains[Argelaguet et al., 2018]. A recently proposed AE-based approach attempts to balance expressive power and interpretability by

combining a non-linear encoder with a linear decoder[Svensson et al., 2020].

The most commonly used modeling framework for yielding an interpretable decomposition of multi-view data are factor analysis models with structured sparsity [Zhao et al., 2016, Klami et al., 2014]. These models result in sparse factor loadings, allowing for a direct inspection and interpretation of each factor from a domain expert.

However, this manual annotation of factors is cumbersome, time consuming and requires highly-specialized expertise.

To automate this annotation process, we propose to leverage the partial knowledge on the structure of the latent space that is readily available in a structured manner in many domains. For example, in genomic medicine, disease states are often characterized by sets of features (or pathways), comprising genes that are known to act in a coordinated manner. These data, collected over many years of scientific progress, are curated in dedicated pathway databases.

However, integrating this domain knowledge in a principled manner as sparsity prior in multi-view models is challenging: domain knowledge is noisy (e.g. pathways contain many false positive and false negative annotations) and domain knowledge is incomplete and often only available for a subset of views (e.g. in genomic medicine pathway information is only readily available for the transcriptome and the genome).

In this work we propose a novel approach for incorporating domain knowledge via structured sparse priors for analysing multi-view data in an inherently explainable manner. Our domain-informed priors render the learnt latent variables directly interpretable without any further interaction with domain expert, by tagging each latent variable with its corresponding feature set (or pathway in genomic medicine).

The contributions of our paper are as follows:

- We develop a **multi-view** latent variable model with domain-informed structured sparsity (MuVI) that integrates noisy domain expertise in terms of feature sets.
- We demonstrate that our model utilizes prior information efficiently by recovering correct signals from noisy feature sets and is robust to poorly specified priors.
- We show that feature-set priors result in identifiable factors, and promote partial identifiability in the uninformed views.

- We demonstrate the practical utility of our model on a large multi-view dataset of cancer patients by inferring interpretable and biologically meaningful axes of variation.

## 2 Related Work

Factor analysis (FA) is a fundamental approach for estimating and understanding the correlation structure among observed variables[Thurstone, 1931], which has inspired the development of numerous latent variable models. Due to its simplicity, however, standard FA is unable to model observations from multiple sources. Extensions, such as the canonical correlation analysis (CCA)[Hotelling, 1992, Klami et al., 2013], or the group factor analysis (GFA)[Klami et al., 2014] model paired observations simultaneously by learning linear dependencies underlying two or more data sources or views. A central assumption of the GFA is that the multi-view observations are a manifestation of a lower dimensional common latent space corrupted by Gaussian noise. The main components that describes this relationship are the factor-to-feature linear mappings or the so-called factor loadings. Factor loadings encode the structure of each factor, and play an important role in the interpretation of the model. Hence, factor loadings are suitable for introducing statistical assumptions on their underlying structure such as sparsity. For instance, GFA quantifies the association between view and factor by extending the automatic relevance determination (ARD)[MacKay et al., 1994]. In non-Bayesian approaches, sparsity is commonly handled by introducing additional terms of an optimization objective posed on the model parameters. A canonical example is the the L1 penalty, also known as the lasso[Tibshirani, 1996]. On the other hand, Bayesian approaches achieve sparse solutions via particular sparsity inducing priors. For instance, the double exponential, or Laplace prior is the Bayesian counterpart of the lasso[Park and Casella, 2008]. Another popular choice is the discrete spike-and-slab prior[Mitchell and Beauchamp, 1988], a mixture of a Dirac delta distribution centered at zero for pruning irrelevant signals, and a normal distribution for modeling larger signals. Recently, the spike-and-slab lasso (SSL)[Ročková and George, 2018] has emerged as a combination of two Laplace distributions that are parameterized to emulate both the spike and the slab component. Other flavours of continuous shrinkage priors[Polson and

Scott, 2010] include the horseshoe prior[Carvalho et al., 2009, 2010], which offers a continuous relaxation of the spike-and-slab approach, thereby preserving sparse properties while providing computational benefits such as being differentiable.

Several Bayesian approaches have successfully utilized the synergy between latent variable models and sparsity inducing priors[Bernardo et al., 2003, Engelhardt and Stephens, 2010, Lan et al., 2014]. In the multi-view setting, [Zhao et al., 2016] propose a hierarchical Bayesian approach for group factor analysis with structured sparsity, facilitated by a cascading three parameter beta prior[Armagan et al., 2011]. The consequences of this addition are twofold, the column-wise sparsity supports the inference of associations between views, while element-wise sparsity encourages feature selection within each individual factor. Multi-omics factor analysis (MOFA)[Argelaguet et al., 2018] assumes a similar structured sparsity in two levels, which is achieved by combining an ARD prior with a spike-and-slab prior. Beyond linear models, there is an array of non-linear modeling approaches that generalize the ideas of linear LVMs and sparse priors to more complex data settings. These include approaches based on variational autoencoder [Ainsworth et al., 2018] or Gaussian Process Latent Variable Models [Damianou et al., 2012]. Such approaches, however, are difficult to interpret in practice and have therefore not received widespread application. For example, in the latter GP-based approach, loading matrices are marginalized out, and cannot be used to identify any physical or biological processes captured by individual factors. To maintain the expressive power of autoencoders and still facilitate the interpretability of linear models, [Svensson et al., 2020] have recently proposed to combine a non-linear encoder with a linear decoder in an autoencoder framework. While this approach was proposed for single data views, extension to the multi-view setting is straight-forward.

Applications of shrinkage priors are not limited to feature selection, and have been successfully applied in other supervised tasks such as model selection in Bayesian neural networks[Ghosh et al., 2019, Louizos et al., 2017].

Typically, before training sparse latent variable models, the prior assumptions are set to be relatively vague and uninformative, allowing only the observations to mold the posterior. An alternative approach is introducing an informed structured sparsity into the model based on external

expertise in the domain of interest. The factorial single-cell latent variable model [Buettnner et al., 2017] attempts to bridge this gap by explicitly integrating, and jointly modeling a collection of domain relevant feature sets such as gene set annotations. The model incorporates and extends the spike-and-slab to be informed by the presence or absence of a feature, and infer pre-labeled latent axes of variation. However, this model is only able to model a single data view and the proposed inference scheme is cumbersome and does not scale to large sample sizes. An orthogonal approach for identifying latent variables corresponding to pathways is the single sample gene set enrichment analysis (ssGSEA) [Barbie et al., 2009], where an absolute enrichment of a pathway in each sample is computed. However, this approach does not account for noisy annotations, treats all pathways as independent and can only be applied to a single data view.

A multi-view approach with structured sparsity that admits prior information in terms of feature sets, and is able to handle partial and potentially noisy priors has not yet been explored.

### 3 Domain-informed multi-view modeling

#### 3.1 Background and notation

Let  $\mathbf{y}_i \in \mathbb{R}^D$  denote a  $D$ -dimensional observation for  $i \in \{1, \dots, N\}$ , and  $G_m \subseteq \{1, \dots, D\}$  describe a mutually disjoint grouping of the features into  $M$  data views, where  $G_p \cap G_q = \emptyset$  for  $p \neq q \in \{1, \dots, M\}$ . For simplicity, we assume a permutation of the features  $D$  such that the first  $D_1$  features belong to  $G_1$ , the second  $D_2$  features to  $G_2$  and so on. As a result, we may rewrite the collection of observations as a matrix  $\mathbf{Y} \in \mathbb{R}^{N \times D}$  comprising  $M$  coupled views  $[\mathbf{Y}^{(1)}, \mathbf{Y}^{(2)}, \dots, \mathbf{Y}^{(M)}]$ , where  $\mathbf{Y} \in \mathbb{R}^{N \times D_m}$ . The main goal is to then represent each observation  $\mathbf{y}_i$  in terms of a low-dimensional set of latent factors  $\mathbf{x}_i \in \mathbb{R}^K, K \ll D$ . The relationship between the observations and the latent factors is described by a set of view-specific factor loadings  $\mathbf{W}^{(m)} \in \mathbb{R}^{D_m \times K}$ . Then, the recipe for the group factor analysis framework posits the following generative process to the observed data,

$$\mathbf{y}_i^{(m)} \sim \mathcal{N} \left( \mathbf{W}^{(m)} \mathbf{x}_i, \mathbf{\Psi}^{(m)} \right) \quad (1)$$

where each latent variable typically follows an isotropic standard normal distribution

$$\mathbf{x}_i \sim \mathcal{N}(\mathbf{0}, \mathbf{I}). \quad (2)$$

The residuals are denoted by  $\Psi^{(m)} = \text{diag}(\sigma^{2(m)})$ , a diagonal matrix storing the marginal variances  $\sigma_j^{2(m)}$  of each variable  $j$  in view  $m$ . Due to conjugacy properties, setting

$$\sigma_j^{2(m)} \sim \Gamma^{-1}(\alpha_\sigma, \beta_\sigma) \quad (3)$$

is a common choice, where  $\Gamma^{-1}(\alpha, \beta)$  describes the inverse-Gamma with shape and scale parameters  $\alpha$  and  $\beta$ . Finally, an important component of GFA is the collection of the factor loadings which applies a linear projection of the latent variable  $\mathbf{x}_i$  to  $\mathbf{y}_i^{(m)}$ . In order to facilitate the interpretability of the factor-to-feature mapping, [Klami et al., 2014] propose a structured sparsity for the columns of  $\mathbf{W}^{(m)}$ , such that each factor falls into two distinct categories. A non-zero factor loading vector  $\mathbf{w}_k^{(m)}$  indicates an active factor  $k$ , while  $\mathbf{w}_k^{(m)} = \mathbf{0}$  an inactive factor  $k$  in view  $m$ . Hence, a factor is either shared across an arbitrary subset of views, or private to a specific view.

### 3.2 MUFI

We follow a similar approach, inspired by the success of the horseshoe prior[Carvalho et al., 2009, 2010], and introduce a *view-factor-local* shrinkage prior on the factor loadings to enable both column-wise and element-wise shrinkage:

$$w_{j,k}^{(m)} \sim \mathcal{N}\left(0, \left(\tau^{(m)} \delta_k^{(m)} \lambda_{j,k}^{(m)}\right)^2\right), \quad (4)$$

where each scale in the hierarchy follows a positive Cauchy distribution,

$$\tau^{(m)} \sim \mathcal{C}^+(0, 1) \quad (5)$$

$$\delta_k^{(m)} \sim \mathcal{C}^+(0, 1) \quad (6)$$

$$\lambda_{j,k}^{(m)} \sim \mathcal{C}^+(0, 1). \quad (7)$$

Each level in the hierarchy contributes to the overall structured sparsity of the factor loadings. In particular,  $\delta_k^{(m)}$  serves as an automatic relevance determination (ARD) mechanism[MacKay et al., 1994] for factor  $k$  in view  $m$ , effectively decoupling this factor from the rest of the views. At the same time,  $\lambda_{j,k}^{(m)}$  acts as a regulator on each individual loading, encouraging the model to seek simpler solutions that describe each factor in terms of

fewer features. However, due to the heavy tails of the Cauchy distribution, weakly identified loadings under the horseshoe prior can easily escape the regularization. To counteract this behaviour, the regularized horseshoe guarantees a non-zero penalty even for large weights[Piironen and Vehtari, 2017]. Concurrently, the regularized parameterization helps integrate prior information about the structure of the latent factors into the model. We update Equation 4 as follows. To simplify notation, we sometimes drop the view-specific superscript  $m$ , which can also be implicitly encoded in  $j$ . Let  $\gamma_{j,k} = \tau \delta_k \lambda_{j,k}$ , then

$$w_{j,k} \sim \mathcal{N}\left(0, \frac{(c_{j,k} \gamma_{j,k})^2}{c_{j,k}^2 + \gamma_{j,k}^2}\right) \quad (8)$$

Note that in Equation 8 the  $c_{j,k}^2$  parameter relates to a specific factor loading rather than being a global parameter as is typically the case. For a relatively large  $c_{j,k}^2 \gg \gamma_{j,k}^2$ ,  $w_{j,k}$  is scaled by a factor of nearly  $\gamma_{j,k}$ , rendering the effect of the additional penalty insignificant, and reinstating the original horseshoe prior. On the other hand, when  $c_{j,k}^2 \ll \gamma_{j,k}^2$ ,  $w_{j,k}$  is scaled by a factor of nearly  $c_{j,k}$ , thus setting an upper bound on corresponding factor loadings. Equivalently, the regularized horseshoe can be seen as a continuous alternative to the discrete spike-and-slab prior[Mitchell and Beauchamp, 1988] with a finite slab width. The inverse-Gamma is a suitable choice as a prior

$$c_{j,k}^2 \sim \Gamma^{-1}(\alpha_c, \beta_c). \quad (9)$$

### 3.3 Integrating Prior Knowledge of Feature Sets

Next, we attempt to integrate prior knowledge in terms of potentially noisy feature sets into our MuVI. A feature set  $\mathbf{I}^D$  is a collection of binary variables  $I_j \in \{0, 1\}$ ,  $j \in \{1, \dots, D\}$ , where  $I_j = 1$  indicates the presence of feature  $j$ , and  $I_j = 0$  its absence. Assume we have substantial knowledge about the underlying structure of the factor loadings in terms of feature sets. That is, for every latent dimension  $k$  and a set of features  $D$  we are given a corresponding feature set  $\mathbf{I}_k^D$ , such that  $w_{j,k} > 0$  if  $I_{j,k} = 1$ , and  $w_{j,k} = 0$  otherwise. Then, the solution to a sparse group factor analysis is trivial. Each latent factor can be seen as a factor-to-feature mapping of the subset of active features determined by the feature set. In terms of Equation 8, this can also be achieved by setting the corresponding slab width  $c_{j,k} \approx 0$ , applying an infinitely large weight decay penalty to

$w_{j,k}$ . In practice, we rarely have access to such pristine ground truth. However, in some cases, we may exploit existing domain knowledge to develop a prior belief about a plausible structure of the factor loadings by accommodating noisy feature sets into our modeling approach. Let  $\tilde{\mathbf{I}}^D$  be a noisy version of a feature set  $\mathbf{I}^D$ , where a subset of the binary variables  $I_Q, Q \subset \{1, \dots, D\}$  has been flipped to generate  $\tilde{\mathbf{I}}^D$ , inserting a non-zero fraction of false positives and false negatives. In order to successfully integrate noisy feature sets into MuVI, we need to relax the regularization penalty introduced by a pre-defined  $c_{j,k}$ , allowing the adaptation of incorrect signals, given sufficient evidence from the data. Subsequently, we scale  $c_{j,k}$  by an auxiliary constant  $0 < \alpha_{j,k} \leq 1$ . A value of  $\alpha_{j,k} = 1.0$  poses no prior penalty to  $w_{j,k}$ , while  $\alpha_{j,k} < 1.0$  leads to a smaller slab width a priori. Consequently, a smaller  $\alpha_{j,k}$  translates to a stronger prior belief. Experiments show that values around  $0.01 \leq \alpha_{j,k} \leq 0.05$  for absent features in a prior collection of feature sets provide the best results on average.

### 3.4 Inference

Finally, the joint model can be written as

$$\begin{aligned} p(\mathbf{Y}, \Theta) &= p(\mathbf{Y}, \mathbf{X}, \mathbf{W}, \Lambda, \Delta, \tau, \mathbf{C}, \Psi) \\ &\quad \times p(\mathbf{Y} | \mathbf{X}, \mathbf{W}, \Psi) p(\Psi) \\ &\quad \times p(\mathbf{X}) p(\mathbf{W} | \Lambda, \Delta, \tau, \mathbf{C}) \\ &\quad \times p(\Lambda) p(\Delta) p(\tau) p(\mathbf{C}), \end{aligned} \quad (10)$$

where  $\Theta = \mathbf{Y}, \mathbf{X}, \mathbf{W}, \Lambda, \Delta, \tau, \mathbf{C}, \Psi$ , and

$$\begin{aligned} \mathbf{Y} &= \left\{ y_{i,j}^{(m)} \right\}, \Psi = \left\{ \sigma_j^{(m)} \right\}, \mathbf{X} = \left\{ x_{i,k} \right\}, \mathbf{W} = \left\{ w_{j,k}^{(m)} \right\} \\ \Lambda &= \left\{ \lambda_{j,k}^{(m)} \right\}, \Delta = \left\{ \delta_k^{(m)} \right\}, \tau = \left\{ \tau^{(m)} \right\}, \mathbf{C} = \left\{ c_{j,k}^{(m)} \right\} \end{aligned}$$

Inference is performed by introducing a fully factorized family of parameterized distributions  $q_\phi(\Theta) = \prod_{\theta \in \Theta} q_\phi(\theta)$  to approximate the intractable posterior  $p(\Theta | \mathbf{Y})$ . We maximize the evidence lower bound with respect to the variational parameters  $\phi$ , which, in return reduces the gap between the true and the approximate posterior in terms of the KL divergence. The family of normal distributions is a natural choice for approximating  $\mathbf{X}$  and  $\mathbf{W}$ , whereas, for the rest of the parameters we assert the log-Normal distribution to ensure positive samples[Ghosh et al., 2018]. The resulting optimization objective

$$\mathcal{L}(\phi) = \mathbb{E}_{q_\phi} [\log p(\mathbf{Y}, \Theta) - \log q_\phi(\Theta)] \quad (11)$$

is amenable to black box stochastic variational inference[Ranganath et al., 2014, Hoffman et al., 2013], which involves sampling from the variational distribution, and taking unbiased but noisy Monte Carlo estimates of the gradient  $\nabla_\phi \mathcal{L}$ . In addition, the reparameterization trick[Kingma and Welling, 2013] further stabilizes the optimization procedure, in which the random variables are expressed as a combination of deterministic variables and external random noise, thereby greatly reducing the variance of the MC estimates. We provide an implementations for optimization using Pyro[Bingham et al., 2019] on GitHub<sup>1</sup>.

## 4 Experiments

We first evaluate different aspects of MuVI empirically on a wide range of simulated settings. Ideally, the model performs well in the following general tasks:

- Learning a meaningful latent representation with low reconstruction loss
- Utilizing prior information efficiently by recovering correct signals from noisy feature sets
- Being robust against poorly specified or entirely incorrect prior information
- Promoting an implicit flow of the prior information from the informed to the uninformed views via the shared factors

We compare our model against three baselines that admit observations across multiple views, and learn a sparse representation of the common latent space: the Bayesian group factor analysis with structured sparsity (BASS)[Zhao et al., 2016], multi-omics factor analysis (MOFA)[Argelaguet et al., 2018] and an interpretable multi-view autoencoder (AE), as a naive multi-view extension to the interpretable autoencoder[Svensson et al., 2020].

Finally, we demonstrate the practical utility of MuVI on a real-world dataset from The Cancer Genome Atlas (TCGA)[Tomczak et al., 2015].

### 4.1 Synthetic Experiments

#### 4.1.1 Data generation

We compile the synthetic data by generating  $N = 200$  samples across four views, each comprising

<sup>1</sup><https://github.com/MLO-lab/MuVI>

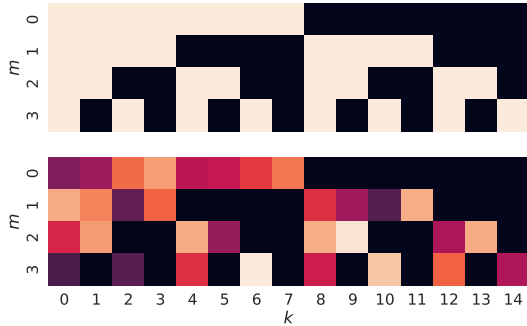


Figure 2: Depiction of cross-view relationships in the synthetic data. True relationship (top) versus inferred relationship based on the factor scales learned by MuVI (bottom).

$D_1 = D_2 = D_3 = D_4 = 400$  features. The latent space consists of  $K = 15$  factors, that are linearly transformed by a set of sparse factor loadings. Each weight is sampled independently from a standard normal distribution, where loadings with an absolute value of less than 0.1 are set to zero, to emphasize the gap between active and inactive signals. In addition, we randomly set 85%–95% of the loadings to zero. The relationship between the data views is explained by the structured sparsity of the loadings. In particular, we generate all combinations of four binary variables, resulting in 15 distinct relationship configurations for each factor as depicted in the top heatmap of Figure 2. A dark entry means the factor does not contribute to the corresponding view, and decouples it from the rest of the views. For instance, factor with index 0 is fully shared across all views, whereas factor 7, 11, 13 and 14 explain variability pertaining to each view individually. The rest of the factors exhibit a mixture of partially shared configurations.

We extract the true factor loadings mask, indicating active and inactive features for each latent dimension, and generate potentially noisy feature sets which serve as prior information during training. We perturb the feature sets by swapping 10%, 20%, 50%, 90% and 100% of the true positives with true negatives. The severity of the noise translates to a poorly specified prior belief, where 100% noise means that the prior belief is entirely incorrect, up to the number of the expected active features. Also, we introduce additional false positives for factors that are inactive, as to further disguise any true underlying relationship within and between views.

	RMSE	Precision	Recall	$F_1$
BASS	$0.543 \pm 0.02$	<b><math>0.944 \pm 0.05</math></b>	$0.899 \pm 0.03$	$0.920 \pm 0.04$
MOFA	$0.331 \pm 0.00$	$0.541 \pm 0.14$	$0.914 \pm 0.02$	$0.672 \pm 0.11$
AE	$0.325 \pm 0.01$	$0.692 \pm 0.06$	$0.964 \pm 0.01$	$0.805 \pm 0.04$
MuVI <sub>–</sub> (uninformed)	<b><math>0.323 \pm 0.00</math></b>	$0.933 \pm 0.05$	<b><math>0.995 \pm 0.00</math></b>	<b><math>0.962 \pm 0.03</math></b>
MuVI <sub>0.5</sub> (1 inf. view)	<b><math>0.322 \pm 0.00</math></b>	$0.966 \pm 0.01$	$0.996 \pm 0.00$	$0.981 \pm 0.00$
MuVI <sub>0.1</sub> (1 inf. view)	<b><math>0.322 \pm 0.00</math></b>	$0.965 \pm 0.01$	$0.997 \pm 0.00$	$0.982 \pm 0.00$
MuVI <sub>0.1</sub> (3 inf. views)	<b><math>0.322 \pm 0.00</math></b>	<b><math>0.974 \pm 0.01</math></b>	<b><math>0.998 \pm 0.00</math></b>	<b><math>0.986 \pm 0.01</math></b>

Table 1: Performance comparison on the synthetic data. Average metric scores across five independent runs  $\pm$  standard deviation.

#### 4.1.2 Evaluation

We evaluate all models on five randomly generated datasets as described above, and report average metric scores across all views. We assess the quality of the representation in terms of RMSE between the true observations and the reconstructed views from the common latent space. We quantify the concordance between the inferred factor loadings and the true underlying structure by reporting the precision, recall and the  $F_1$  score. As a prerequisite to calculating the binary scores we extract a binary representation of active and inactive features based on a threshold. For our model and MOFA, the threshold of 0.1 matches the true cutoff between active and inactive signals when generating the sparse loadings. For BASS and AE, the optimal thresholds were 0.05 and 0.01, respectively. Moreover, since the factor analysis suffers from non-identifiability[Shapiro, 1985], a matching of the latent factors and their corresponding factor loadings is necessary. However, we highlight that this issue is less severe for the latent structure learned by our model, and later show that the structure reinforced by the prior information is, under certain conditions, identifiable.

#### 4.1.3 Training

The parameter and training settings for the baselines are summarized in the Appendix A. We perform a grid search on the single hyperparameter of MuVI, the auxiliary constants  $\alpha_{j,k}$  for the factor loadings that are not part of the prior feature sets. Among  $\{0.01, 0.03, 0.05, 0.1\}$ ,  $\alpha_{j,k} = 0.03$  reliably performs the best. We train several models with different noise configuration and prior information availability. We start with an uninformed model and iteratively increase the amount of the prior information by informing a single view, two views and eventually three views. An important consideration when injecting prior information for a subset of views is assuming that the features

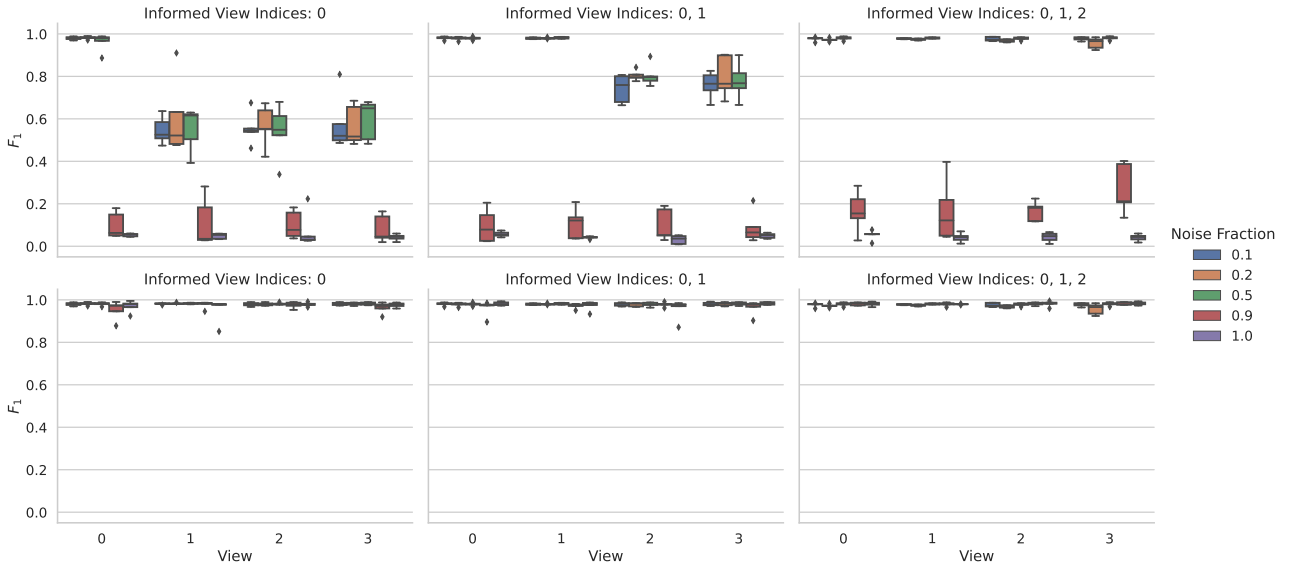


Figure 3: Performance across multiple prior noise configurations and prior information availability. Raw results of the unmatched factors (top) versus the results after the corrected order in a post processing step (bottom). Each boxplot summarizes five independent runs of the same configuration.

of the rest of the views are not present in the prior feature sets, and informing them accordingly. In other words, we choose the same  $\alpha_{j,k}$  for all the factor loadings for the uninformed views that we choose for the factor loadings of the informed views that are absent in the prior feature sets. The main rationale behind this decision is encouraging the informed views to learn first, and gradually inform the rest of the uninformed views implicitly via the structure of the shared factors. Also, we observed empirically that the uninformed views are unrestricted in terms of learning and typically converge very early during training and are unable to “unlearn” a suboptimal structure of the factor loadings.

#### 4.1.4 Results

We provide a visual summary of the experiments in Figure 1, and a detailed overview of the metric scores in Table 1. We first notice a difference in the quality of the latent representation, measured by the RMSE. MuVI, MOFA and the autoencoder (AE) perform comparably well. BASS appears to sacrifice reconstruction quality in favor of additional sparsity, which is supported by a very high precision and relatively lower recall. Our modelling approach, on the other hand, strikes a better balance between learning a good latent representation with low reconstruction error and pruning away the majority of superfluous connections between the latent factors and the observed features. In addition, the high recall indicates a better ca-

pability of MuVI to retrieve almost all positive signals, at the cost of some redundant signals. In addition to the uninformed version of our model, we report the results for three additional model configurations. The first model simulates a realistic scenario when the available information is very limited and noisy. Specifically, we inform only the first view with highly perturbed feature sets with a noise fraction of 50%. Compared to the uninformed MuVI model, we notice an increase the precision, while the recall remains intact, thereby further improving the  $F_1$ . In the next two models, we first reduce the amount of noise to 10%, then increase the number of informed views to 3. We observe additional improvements in all three binary scores, which further emphasizes the benefit of increasing the quality and the quantity of the prior information.

Next, we assess the robustness of MuVI against severe noise, and its capability of utilizing useful prior information to infer a corrected latent representation. Figure 3 depicts a comprehensive overview of the results across multiple training settings. In the top row we show the results for the unmatched factors, whereas in the bottom row the factors underwent a permutation post training to match the true order. For a fair comparison, since all baselines are completely unidentifiable and require factor matching, the scores reported in Table 1 also originate from the bottom row. On the common horizontal axes, from left to right, we increase the number of views that are informed

starting with a single view in the first column, first and second view in the middle column, and the first three views in the last column. Within each subplot, the results are computed and documented separately for each view. Finally, each group of view-specific boxplots is ordered by the fraction of prior noise in ascending order. We notice several attributes of our model. First, MuVI exhibits no difficulties in learning a good representation from mild to moderate noise in the prior information. As expected, a severe perturbation reduces the ability of our model to find the proper ordering of the factors dramatically. However, the bottom row provides evidence that the model merely loses its ability to be identifiable, since the quality of the representation remains virtually intact. To further reinforce the idea of partial identifiability offered by our model, notice the increase in the  $F_1$  score when moving along the subplots from left to right, that is, increasing the number of informed views. The informed factors serve as anchors in the overall ordering, while at the same time decreasing the number of possible permutations available for potentially uninformed or view-specific factors. The effect of the prior information is noticeable not only within each informed view, but also across the combined observations. For instance, the uninformed views in the first column, i.e. 1, 2 and 3, fluctuate around an  $F_1$  score of 0.65, if we ignore the results with severe noise of 90% and 100%. In the second and the third column, the results for the uninformed views alone improve significantly, which suggests that the shared factors are capable of correctly transferring their prior information among the uninformed views.

Finally, we look at the ability of MuVI to communicate the underlying relationship between the views. The bottom heatmap in Figure 2 corresponds to the MAP estimates of the factor scales  $\delta_k^{(m)}$  learned during inference. The model successfully learns to turn off irrelevant factors and highlights cross-view relationships by assigning large positive values to active and shared factors, thereby diminishing the regularization penalty imposed by the sparse prior.

## 4.2 The Cancer Genome Atlas (TCGA)

We investigate a large dataset of comprehensive multi-omic profiling of over 11 thousand samples from 33 cancer types[Tomczak et al., 2015]. Each sample comprises sets of features of various sizes across four biologically distinct views: DNA

methylation, mRNA expression, microRNA expression and reverse phase protein array (RPPA). We include a preprocessing step of centering the data and standardizing each view globally due to the large discrepancy in value ranges across different views. In addition, samples exhibit partial or complete missingness in individual views, which we accommodate in our modeling approach. Prior to training MuVI on the TCGA data, we derive a collection of gene set annotations (acting as feature sets) from curated public databases such as MSigDB[Liberzon et al., 2015], Reactome[Fabregat et al., 2018] and KEGG[Kanehisa and Goto, 2000]. A gene set consists of a group of genes that are biologically meaningful when co-expressed under certain conditions, or describe functionally distinct pathways in biological systems. As informative prior we consider gene set annotations where at least 15 genes were present in the data, resulting in 360 annotations with a median size of 30. Since gene sets encompass only genomic and transcriptomic features, we are limited to informing only the first two views, namely the DNA and the mRNA. We take advantage of the stochastic variational inference algorithm and propagate batches of 1,000 samples during training. The algorithm terminates when the optimization objective no longer improves based on the difference between consecutive iterations, and after a certain number of patience steps. Training converges in less than 12 minutes on a single NVIDIA Quadro RTX 5000 GPU with 16 GB memory.

In Figure 4 we display a summary of the results on the TCGA dataset. First, we assess the quality of the latent representation inferred by our model. We apply a t-distributed stochastic neighbor embedding (t-SNE) approach to further compress the latent space into two dimensions for better visualization[Van der Maaten and Hinton, 2008]. In the left we plot the new embeddings, colored by their corresponding cancer type. The model is able to learn a meaningful structure by grouping cancer patients of a similar type closer together. Next, we explore individual latent factors to gain more insights into the main drivers of heterogeneity with respect to particular cancer types. Melanogenesis (K) from the KEGG collection and the androgen response (H) from the hallmark collection describe general biological processes. Melanogenesis describes the process of producing the melanin pigments from melanocytes, commonly found in the epidermis and hair follicles. Androgen response orchestrates the activation of male hormone re-

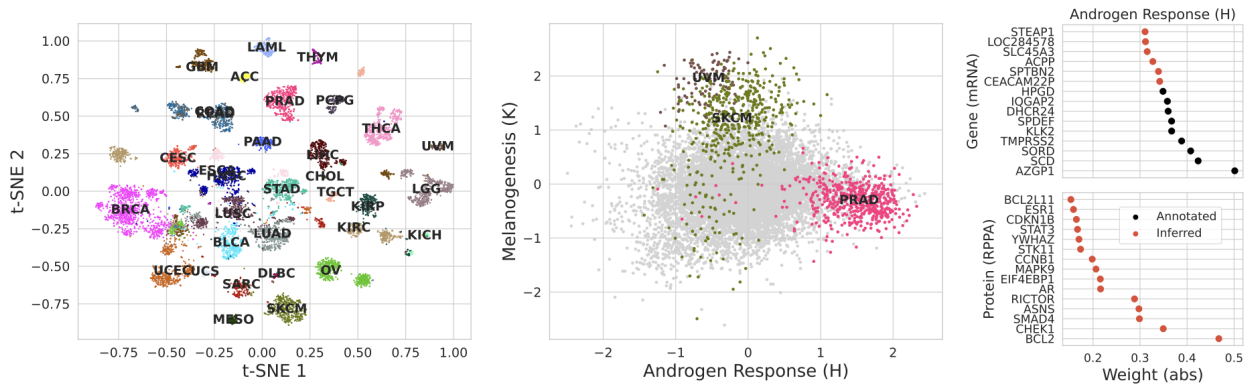


Figure 4: Results of the TCGA dataset. A t-SNE embedding space learned from the latent representation of MuVI (left). Inferred latent factors that are informed by androgen response and melanogenesis a priori (center). Top 15 features based on the absolute value of their corresponding factor loadings for the shared androgen response factor among mRNA and RPPA (right).

ceptors, and plays an important role in the development and progression of prostate cancer[Fujita and Nonomura, 2019]. In the middle of Figure 4 we illustrate a scatter plot by mapping our samples onto the two latent axes informed and described by androgen response and melanogenesis. We highlight three cancer types with the same coloring as the previous t-SNE plot, while fading the remaining 30 cancer types to gray. As anticipated, melanogenesis helps identify the only two groups of samples from tissues with skin cutaneous melanoma (SKCM) and uveal melanoma (UVM). Likewise, androgen response assigns significantly higher scores to patients with prostate adenocarcinoma (PRAD). Next, in the rightmost plots, we dive one level deeper and inspect the top 15 features of the androgen response factor, which is active and shared among the mRNA and the RPPA view. We decide whether a factor is active in view  $m$  if its corresponding factor scale is not virtually zero, i.e.  $\delta_k^{(m)} > 0.01$ , as well as if the variance explained by the factor exceeds a threshold of 0.5%, based on the coefficient of determination  $R^2$ . We reiterate that we informed only mRNA among the two views. Hence, we expect to see annotated genes weighted highly based on the absolute value of their corresponding factor loading. A powerful feature of MuVI is the refinement of provided feature sets by adding or removing features in a data-driven manner. Investigating inferred genes for the Androgen Response factor, we discover several previously known biomarkers of clinical relevance such as STEAP1, SLC45A3[Perner et al., 2013] and ACPP. The six-transmembrane epithelial antigen of the prostate 1 (STEAP1) is overexpressed in prostate cancer and serves

as a diagnostic and prognostic biomarker[Khanna et al., 2021]. Also, it has been shown that levels of ACPP or prostatic specific acid phosphatase (PSAP), increase with prostate cancer progression[Kong and Byun, 2013]. We now move on to the uninformed view, where we expect the androgen response factor of mRNA to influence the structure of the factor loadings in the RPPA, such that the inferred factor reveals additional biomarkers linked to prostate cancer. Based on the amount of variance explained by this factor in the RPPA view, and the significance of the shared and informed factor from the mRNA view, we have strong evidence about the association of the top proteins with the disease. For example, inferred BCL2 is an oncogene that inhibits the process of apoptosis, or the process of programmed cell death. It has been demonstrated that BCL2 is a prerequisite for the progression of cancer cells from an androgen-dependent stage, the earlier stages of the cancer progression, to an androgen-independent growth stage[Lin et al., 2007]. Moreover, therapeutic approaches that target the checkpoint kinase 1 (CHEK1) have demonstrated favorable clinical outcomes for prostate cancer patients[Drápela et al., 2020].

## 5 Conclusion and Discussion

In this contribution, we have addressed the task of modeling multi-view data with interpretable latent variable models. We use a Bayesian approach with structured sparsity to encode domain knowledge in the priors of a factor analysis model. Our model is able to integrate noisy domain expertise and results in factors that are inherently inter-

pretable via their pre-defined feature sets. In contrast to other sparse multi-view models, our approach is able to recover correct signals from noisy feature sets, while maintaining a low reconstruction error.

We demonstrate in a real-world application that our model is able to infer clinically meaningful subpopulations of cancer patients.

## References

Samuel K Ainsworth, Nicholas J Foti, Adrian KC Lee, and Emily B Fox. oi-vae: Output interpretable vaes for nonlinear group factor analysis. In *International Conference on Machine Learning*, pages 119–128. PMLR, 2018.

Ricard Argelaguet, Britta Velten, Damien Arnol, Sascha Dietrich, Thorsten Zenz, John C Marioni, Florian Buettner, Wolfgang Huber, and Oliver Stegle. Multi-omics factor analysis—a framework for unsupervised integration of multi-omics data sets. *Molecular systems biology*, 14(6):e8124, 2018.

Artin Armagan, Merlise Clyde, and David Dunson. Generalized beta mixtures of gaussians. *Advances in neural information processing systems*, 24, 2011.

David A Barbie, Pablo Tamayo, Jesse S Boehm, So Young Kim, Susan E Moody, Ian F Dunn, Anna C Schinzel, Peter Sandy, Etienne Meylan, Claudia Scholl, et al. Systematic rna interference reveals that oncogenic kras-driven cancers require tbk1. *Nature*, 462(7269):108–112, 2009.

JM Bernardo, MJ Bayarri, JO Berger, AP Dawid, D Heckerman, AFM Smith, and M West. Bayesian factor regression models in the “large p, small n” paradigm. *Bayesian statistics*, 7: 733–742, 2003.

Eli Bingham, Jonathan P Chen, Martin Jankowiak, Fritz Obermeyer, Neeraj Pradhan, Theofanis Karaletsos, Rohit Singh, Paul Szerlip, Paul Horsfall, and Noah D Goodman. Pyro: Deep universal probabilistic programming. *The Journal of Machine Learning Research*, 20(1):973–978, 2019.

Florian Buettner, Naruemon Pratanwanich, Davis J McCarthy, John C Marioni, and Oliver Stegle. f-sclvm: scalable and versatile factor analysis for single-cell rna-seq. *Genome biology*, 18(1):1–13, 2017.

Yanshuai Cao and David J Fleet. Generalized product of experts for automatic and principled fusion of gaussian process predictions. *arXiv preprint arXiv:1410.7827*, 2014.

Carlos M Carvalho, Nicholas G Polson, and James G Scott. Handling sparsity via the horseshoe. In *Artificial Intelligence and Statistics*, pages 73–80. PMLR, 2009.

Carlos M Carvalho, Nicholas G Polson, and James G Scott. The horseshoe estimator for sparse signals. *Biometrika*, 97(2):465–480, 2010.

AC Damianou, Carl Henrik Ek, MK Titsias, and ND Lawrence. Manifold relevance determination. In *29th International Conference on Machine Learning, ICML 2012, 26 June 2012 through 1 July 2012, Edinburgh*, pages 145–152, 2012.

Stanislav Drápela, Prashant Khirsariya, Wytske M van Weerden, Radek Fedr, Tereza Suchánková, Diana Búzová, Jan Červený, Aleš Hampl, Martin Puhr, William R Watson, et al. The chk1 inhibitor mu380 significantly increases the sensitivity of human docetaxel-resistant prostate cancer cells to gemcitabine through the induction of mitotic catastrophe. *Molecular oncology*, 14(10):2487–2503, 2020.

Barbara E Engelhardt and Matthew Stephens. Analysis of population structure: a unifying framework and novel methods based on sparse factor analysis. *PLoS genetics*, 6(9):e1001117, 2010.

Antonio Fabregat, Steven Jupe, Lisa Matthews, Konstantinos Sidiropoulos, Marc Gillespie, Phani Garapati, Robin Haw, Bijay Jassal, Florian Korninger, Bruce May, et al. The reactome pathway knowledgebase. *Nucleic acids research*, 46(D1):D649–D655, 2018.

Kazutoshi Fujita and Norio Nonomura. Role of androgen receptor in prostate cancer: a review. *The world journal of men’s health*, 37(3):288–295, 2019.

Soumya Ghosh, Jiayu Yao, and Finale Doshi-Velez. Structured variational learning of bayesian neural networks with horseshoe priors. In *International Conference on Machine Learning*, pages 1744–1753. PMLR, 2018.

Soumya Ghosh, Jiayu Yao, and Finale Doshi-Velez. Model selection in bayesian neural networks via horseshoe priors. *J. Mach. Learn. Res.*, 20(182):1–46, 2019.

Matthew D Hoffman, David M Blei, Chong Wang, and John Paisley. Stochastic variational inference. *Journal of Machine Learning Research*, 2013.

Harold Hotelling. Relations between two sets of variates. In *Breakthroughs in statistics*, pages 162–190. Springer, 1992.

Minoru Kanehisa and Susumu Goto. Kegg: kyoto encyclopedia of genes and genomes. *Nucleic acids research*, 28(1):27–30, 2000.

Karan Khanna, Nikki Salmond, Kalan S Lynn, Hon S Leong, and Karla C Williams. Clinical significance of steep1 extracellular vesicles in prostate cancer. *Prostate cancer and prostatic diseases*, 24(3):802–811, 2021.

Diederik P Kingma and Max Welling. Auto-encoding variational bayes. *arXiv preprint arXiv:1312.6114*, 2013.

Arto Klami, Seppo Virtanen, and Samuel Kaski. Bayesian canonical correlation analysis. *Journal of Machine Learning Research*, 14(4), 2013.

Arto Klami, Seppo Virtanen, Eemeli Leppäaho, and Samuel Kaski. Group factor analysis. *IEEE transactions on neural networks and learning systems*, 26(9):2136–2147, 2014.

Hoon Young Kong and Jonghoe Byun. Emerging roles of human prostatic acid phosphatase. *Biomolecules & therapeutics*, 21(1):10, 2013.

Andrew S Lan, Andrew E Waters, Christoph Studer, and Richard G Baraniuk. Sparse factor analysis for learning and content analytics. *The Journal of Machine Learning Research*, 15(1):1959–2008, 2014.

Changhee Lee and Mihaela van der Schaar. A variational information bottleneck approach to multi-omics data integration. In *International Conference on Artificial Intelligence and Statistics*, pages 1513–1521. PMLR, 2021.

Arthur Liberzon, Chet Birger, Helga Thorvaldsdóttir, Mahmoud Ghandi, Jill P Mesirov, and Pablo Tamayo. The molecular signatures database hallmark gene set collection. *Cell systems*, 1(6):417–425, 2015.

Yuting Lin, Junichi Fukuchi, Richard A Hiipakka, John M Kokontis, and Jialing Xiang. Up-regulation of bcl-2 is required for the progression of prostate cancer cells from an androgen-dependent to an androgen-independent growth stage. *Cell research*, 17(6):531–536, 2007.

Christos Louizos, Karen Ullrich, and Max Welling. Bayesian compression for deep learning. *Advances in neural information processing systems*, 30, 2017.

David JC MacKay et al. Bayesian nonlinear modeling for the prediction competition. *ASHRAE transactions*, 100(2):1053–1062, 1994.

Toby J Mitchell and John J Beauchamp. Bayesian variable selection in linear regression. *Journal of the american statistical association*, 83(404):1023–1032, 1988.

Trevor Park and George Casella. The bayesian lasso. *Journal of the American Statistical Association*, 103(482):681–686, 2008.

Sven Perner, Niels J Rupp, Martin Braun, Mark A Rubin, Holger Moch, Manfred Dietel, Nicolas Wernert, Klaus Jung, Carsten Stephan, and Glen Kristiansen. Loss of slc45a3 protein (prostein) expression in prostate cancer is associated with slc45a3-erg gene rearrangement and an unfavorable clinical course. *International journal of cancer*, 132(4):807–812, 2013.

Juho Piironen and Aki Vehtari. Sparsity information and regularization in the horseshoe and other shrinkage priors. *Electronic Journal of Statistics*, 11(2):5018–5051, 2017.

Nicholas G Polson and James G Scott. Shrink globally, act locally: Sparse bayesian regularization and prediction. *Bayesian statistics*, 9(501-538):105, 2010.

Rajesh Ranganath, Sean Gerrish, and David Blei. Black box variational inference. In *Artificial intelligence and statistics*, pages 814–822. PMLR, 2014.

Veronika Ročková and Edward I George. The spike-and-slab lasso. *Journal of the American Statistical Association*, 113(521):431–444, 2018.

Alexander Shapiro. Identifiability of factor analysis: Some results and open problems. *Linear Algebra and its Applications*, 70:1–7, 1985.

Valentine Svensson, Adam Gayoso, Nir Yosef, and Lior Pachter. Interpretable factor models of single-cell rna-seq via variational autoencoders. *Bioinformatics*, 36(11):3418–3421, 2020.

Louis Leon Thurstone. Multiple factor analysis. *Psychological review*, 38(5):406, 1931.

Robert Tibshirani. Regression shrinkage and selection via the lasso. *Journal of the Royal Statistical Society: Series B (Methodological)*, 58(1):267–288, 1996.

Katarzyna Tomczak, Patrycja Czerwińska, and Maciej Wiznerowicz. The cancer genome atlas (tcga): an immeasurable source of knowledge. *Contemporary oncology*, 19(1A):A68, 2015.

Laurens Van der Maaten and Geoffrey Hinton. Visualizing data using t-sne. *Journal of machine learning research*, 9(11), 2008.

Shiwen Zhao, Chuan Gao, Sayan Mukherjee, and Barbara E Engelhardt. Bayesian group factor analysis with structured sparsity. *The Journal of Machine Learning Research*, 2016.

## A Appendix A

The parameter and training settings for the baselines are provided here. We train MOFA combining the ARD and the spike-and-slab prior on the weights for column-wise and element-wise sparsity and apply BASS with default parameters and 20 parameter-expanded expectation maximization (PX-EM) iterations. The autoencoder consists of an encoder-decoder pair for each observed view, connected via a common latent space governed by a product of experts (PoE) approach[Lee and van der Schaar, 2021, Cao and Fleet, 2014]. The encoders comprise two hidden layers of size 64 and 32, each followed by a ReLU activation, whereas the decoders perform a linear mapping of the latent code to the observed features of each view. To achieve sparsity in the factor-to-feature mapping, we introduce an L1 penalty term in the respective decoder weights.

## B Appendix B

We assessed the effect of the threshold on precision and recall by generating PR curves. Figure 5 depicts the precision-recall curves for all models.

## C Appendix C

Here, we show that our approach is robust to the choice of the single hyperparameter  $\alpha$ . Figure 6 compiles the results of a hyperparameter sensitive analysis for the synthetic experiments in Section 4.1.

## D Appendix D

Finally, we show in Figure 7 that an autoencoder does not capture any additional information than MuVI in the latent space in terms of identifying subpopulations.

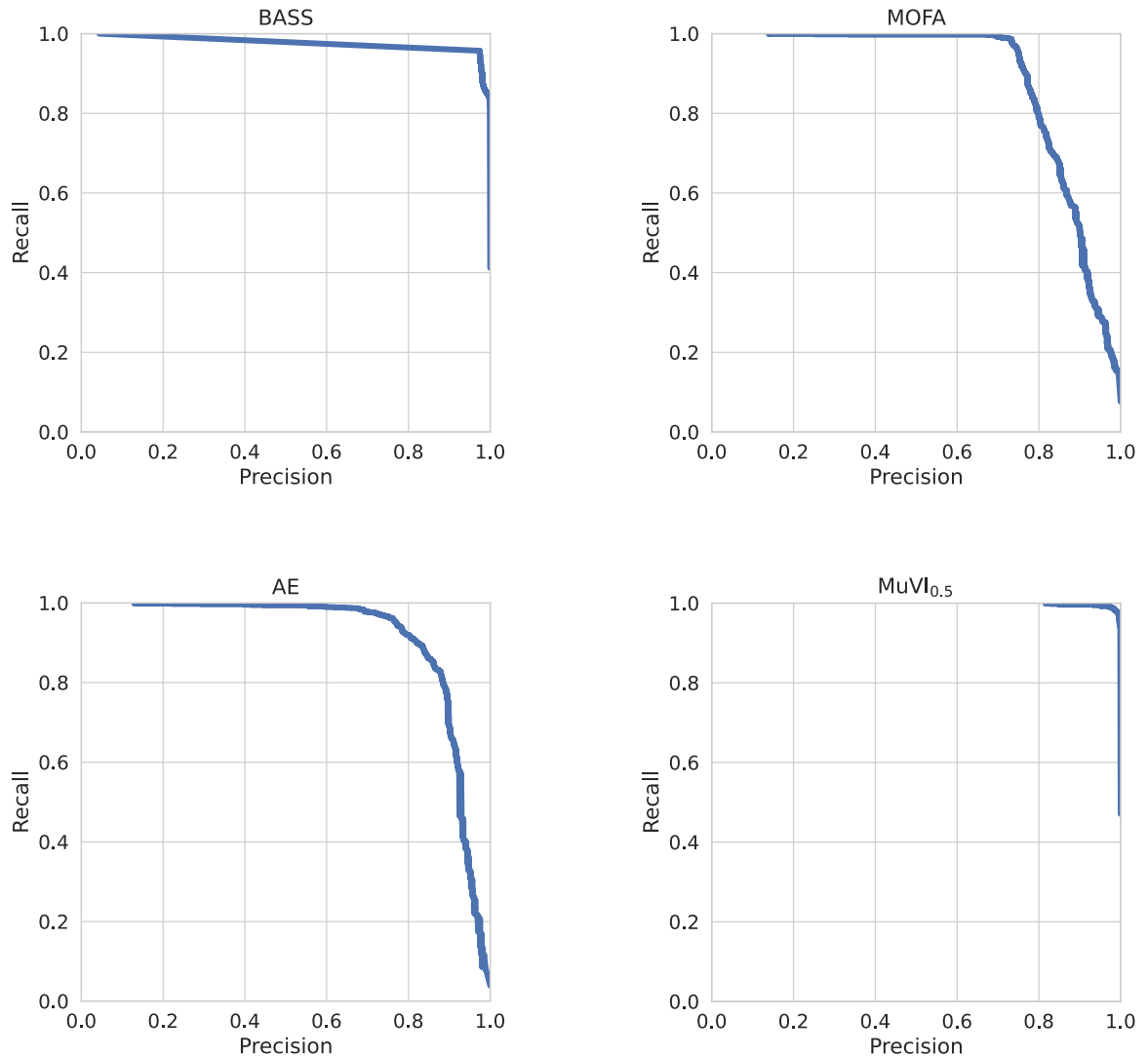


Figure 5: Precision-recall curves for MuVI<sub>0.5</sub> and the baseline models: BASS, MOFA, AE.

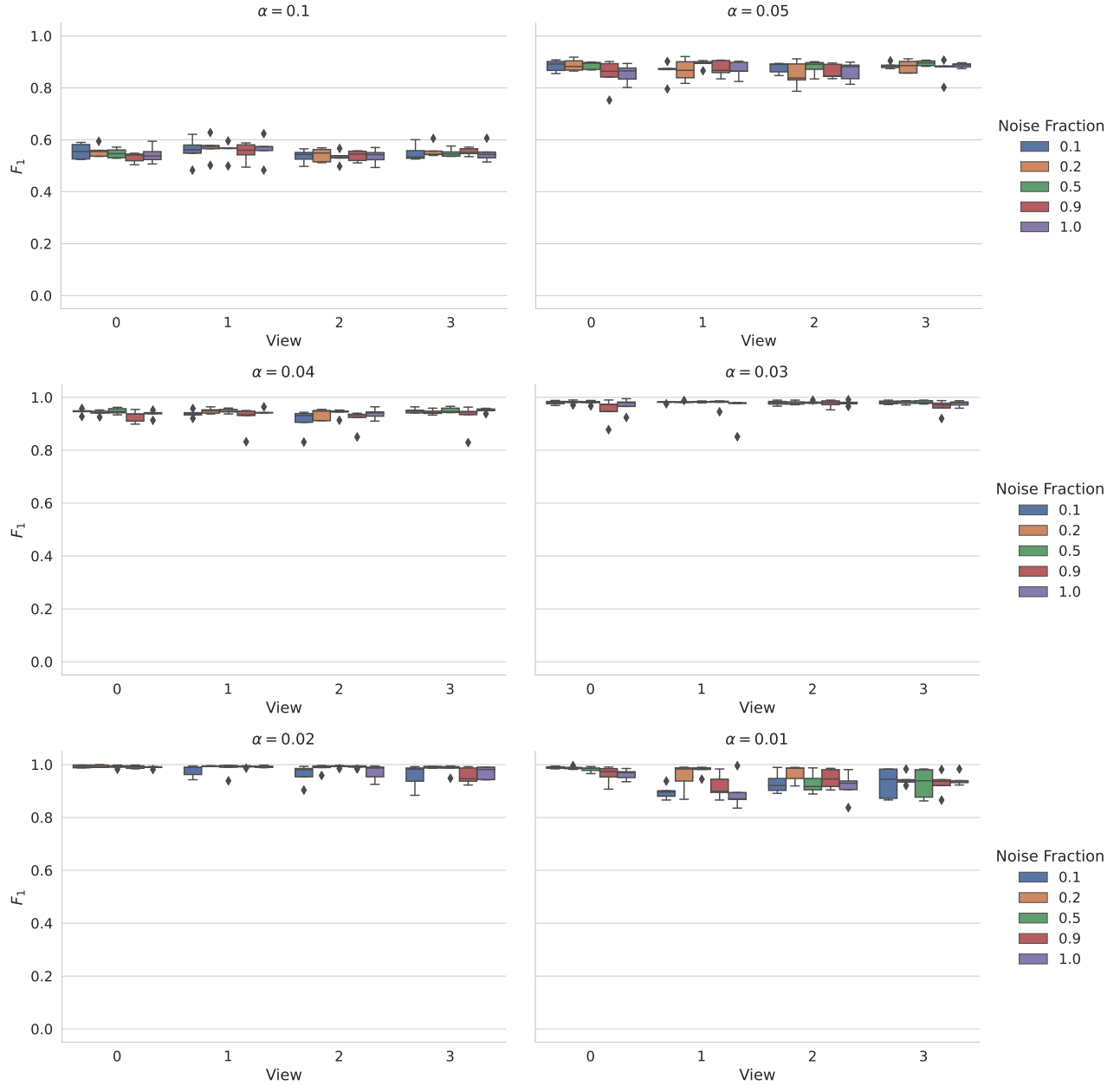


Figure 6: Sensitivity analysis to the auxiliary  $\alpha_{j,k}$  set to inactive signals in the prior feature set. Results when informing only the first view.

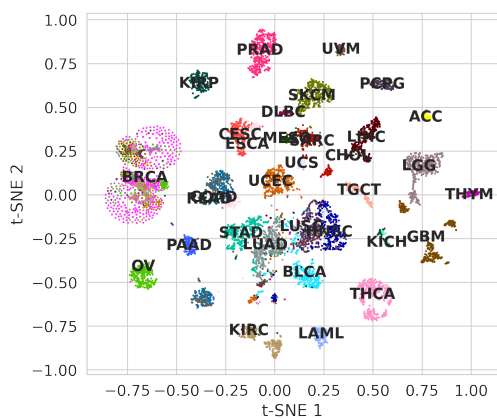


Figure 7: Embedding space learned by the hybrid autoencoder.